Science of the Total Environment 932 (2024) 172934

Contents lists available at ScienceDirect

Science of the Total Environment

journal homepage: www.elsevier.com/locate/scitotenv

Understanding the dynamics of enhanced light non-aqueous phase liquids (LNAPL) remediation at a polluted site: Insights from hydrogeophysical findings and chemical evidence

Paolo Ciampi [a,f,*], Giorgio Cassiani [b], Gian Piero Deidda [c], Carlo Esposito [a,f], Paolo Rizzetto [d], Andrea Pizzi [d], Marco Petrangeli Papini [e,f]

[a] Department of Earth Sciences, Sapienza University of Rome, Piazzale Aldo Moro 5, 00185 Rome, Italy
[b] Department of Geosciences, University of Padua, Via Gradenigo 6, 35131 Padua, Italy
[c] Department of Civil, Environmental Engineering and Architecture, University of Cagliari, via Marengo, 2, 09123 Cagliari, Italy
[d] Logistic Headquarter of Italian Air Force, Viale dell'Università, 4, 00185 Rome, Italy
[e] Department of Chemistry, Sapienza University of Rome, Piazzale Aldo Moro 5, 00185 Rome, Italy
[f] CERI Research Center, Sapienza University of Rome, Piazzale Aldo Moro 5, 00185 Rome, Italy

HIGHLIGHTS

- Electrical resistivity tomography (ERT) enables real-time monitoring of remediation.
- ERT dynamically visualizes migration pathways of reagents and contaminant mobilization.
- Chemical monitoring reveals effective mobilization of aged and residual hydrocarbons.
- Overlap of geophysical-chemical evidence deepens understanding of contaminant behavior.
- The approach offers deep insights into subsurface complexity, advancing remediation.

GRAPHICAL ABSTRACT

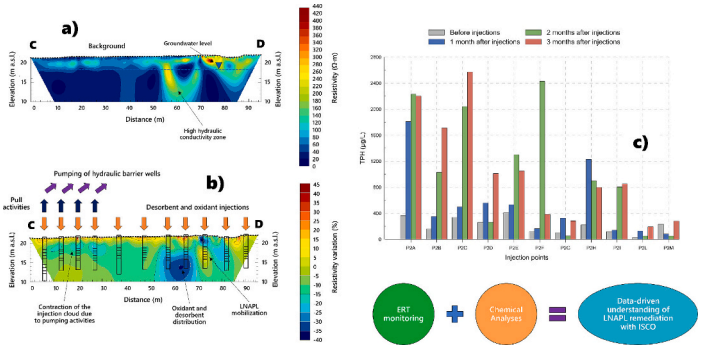

ARTICLE INFO

Editor: Frederic Coulon

Keywords:
Electrical resistivity tomography
Hydrogeophysics
Light non-aqueous phase liquids
Groundwater
Remediation
In-situ chemical oxidation

ABSTRACT

This study intricately unfolds a pioneering methodology for remediating contaminants in a persistent light non-aqueous phase liquids (LNAPL)-contaminated site. The remediation strategy seamlessly integrates enhanced desorption and in-situ chemical oxidation (ISCO), orchestrating the injection of PetroCleanze® (a desorbent) and RegenOx® (an oxidizer) through meticulously designed wells. These injections, based on detailed geological and hydrogeological assessments, aim at mobilizing residual contaminants for subsequent extraction. Real-time subsurface dynamics are investigated through geophysical monitoring, employing electrical resistivity tomography (ERT) to trace reagent migration pathways via their effect on bulk electrical conductivity. The integration of groundwater sampling data aims at providing additional insights into the transformations of contaminants in the spatiotemporal context. Vivid two-dimensional time-lapse ERT sections showcase the evolution of resistivity

* Corresponding author at: Department of Earth Sciences, Sapienza University of Rome, Piazzale Aldo Moro 5, 00185 Rome, Italy.
E-mail addresses: paolo.ciampi@uniroma1.it (P. Ciampi), giorgio.cassiani@unipd.it (G. Cassiani), gpdeidda@unica.it (G.P. Deidda), carlo.esposito@uniroma1.it (C. Esposito), paolo.rizzetto@am.difesa.it (P. Rizzetto), andrea.pizzi@aeronautica.difesa.it (A. Pizzi), marco.petrangelipapini@uniroma1.it (M.P. Papini).

https://doi.org/10.1016/j.scitotenv.2024.172934
Received 28 February 2024; Received in revised form 22 April 2024; Accepted 30 April 2024
Available online 3 May 2024

anomalies, providing high-resolution evidence of the heterogeneity, dispersion pathways of desorbent and oxidant, and residual LNAPL mobilization. Hydrochemical analyses complement this, revealing effective mobilization processes with increasing aqueous concentrations of total petroleum hydrocarbons (TPH) over time. Speciation analysis unveils the intricate interplay of desorption and oxidation, portraying the dynamic fractionation of hydrocarbon components. The hydrogeophysical and data-driven framework not only delivers qualitative and quantitative insights into reagent and contaminant distribution but also enhances understanding of spatial and temporal physio-chemical changes during the remediation process. Time-lapse ERT visually narrates the reagent's journey through time, while chemical analyses depict the unfolding processes of desorption and oxidation across space and time. The coupling of hydrogeophysical and chemical findings pictures the transformations of pollutants following the sequence of product injection and the push and pull activities, capturing the removal of mobilized contaminants through hydraulic barrier wells. This enhanced understanding proves instrumental towards optimizing and tailoring remediation efforts, especially in heterogeneous environmental settings. This study establishes a new standard for a sophisticated and innovative contaminant remediation approach, advancing environmental practices through the harmonized analysis of geophysical and chemical data.

1. Introduction

1.1. Evolutionary contamination scenarios for sites affected by petroleum hydrocarbons

The remediation of areas contaminated by petroleum hydrocarbons, such as diesel, gasoline, and jet fuel, poses an increasingly daunting global challenge (Kuppusamy et al., 2020; Ossai et al., 2020). These compounds fall under the category of light non-aqueous phase liquids (LNAPL) and comprise complex mixtures of hydrocarbons with significantly diverse chemical, physical, and biodegradation properties (Ismail et al., 2023). Due to their intricate interactions with geological and environmental conditions, managing and remediating LNAPL-impacted sites presents inherent challenges (Ebrahimi et al., 2019). The geometrical architecture of LNAPL distribution reflects the migration of spilled products into the unsaturated domain due to gravity, lateral spreading while floating on the water table surface, redistribution of residual product through fluctuating groundwater levels, trapping of residual phase in saturated and unsaturated zones, volatilization dynamics, mobilization/dissolution, and biodegradation of LNAPL, all under the control of the often important system's heterogeneities (Cavelan et al., 2022; Ismail et al., 2023; Lari et al., 2018; Teramoto et al., 2020; Tomlinson et al., 2017). These dynamics result in the natural aging of petroleum hydrocarbons in contaminated sites, leading to the chemical sequestration and physical entrapment of these hydrophobic compounds (Gatsios et al., 2018; Teramoto et al., 2020). The progressive aging of hydrocarbons corresponds to a reduction in the more mobile and degradable fractions, coupled with an increase in compounds with higher molecular weight. These immobile, less volatile, less soluble, more viscous, and high molecular weight materials constitute a persistent secondary source of residual hydrocarbons, originating a plume through the dissolution of its components. This immobile phase is practically impossible to mobilize using traditional extraction technologies (i.e., pumping) (Lari et al., 2018; Ossai et al., 2020). The aging or weathering process can cause modifications that are crucial to consider when selecting a remediation technique, making it an essential aspect of managing polluted sites.

1.2. Remediation strategies for groundwater contaminated with LNAPL: a spotlight on in situ chemical oxidation (ISCO)

Various remediation methods, including on-site techniques such as pump and treat (P&T) and ultraviolet oxidation, and in-situ techniques such as groundwater sparging, air stripping, activated carbon treatment, chemical oxidation (ISCO), bioremediation, and permeable reactive barriers (PRB), have been identified as potentially effective approaches for addressing groundwater contaminated with petroleum hydrocarbons (Fan et al., 2017; Kuppusamy et al., 2020). While conventional strategies such as P&T may overlook secondary environmental burdens and socioeconomic impacts, sustainable remediation technologies such as low-impact bioremediation, innovative forms of in-situ chemical treatment, and passive barriers have the potential to significantly reduce the environmental footprint of remediation and maximize overall net benefits (Brusseau and Guo, 2014; Ciampi et al., 2023; Faisal et al., 2018; Hou et al., 2023; Mackay and Cherry, 1989). Among these, ISCO stands out as a crucial tool for remediating contaminated groundwater, especially when integrated into a comprehensive approach for addressing large and complex sites (Pac et al., 2019; Ranc et al., 2016; Wang et al., 2013; Zhou et al., 2019). However, technical challenges related to hydrogeologic heterogeneities, limitations in oxidant distribution, highly contaminated zones, and contamination in low permeable zones may result in rebound and slow contaminant removal during post-oxidant injection groundwater monitoring (Ghosh et al., 2019; Huling et al., 2017). To enhance the recovery of sorbed-phase or smeared hydrocarbons and improve the solubilization and mass transfer of strongly adsorbed hydrophobic organic compounds in porous media, chemicals can be combined with ISCO (Besha et al., 2018; Wang et al., 2013; Sharma et al., 2020; Barbati et al., 2023). The literature emphasizes the critical importance of understanding subsurface heterogeneity for the effective delivery of an ISCO reagent (Pac et al., 2019).

1.3. Advancing polluted site investigation: hydrogeophysical tools for characterization and monitoring of remediation strategies

Typical investigation and characterization methods for sites contaminated with LNAPLs often rely on point sampling through soil cores or monitoring wells (Algreen et al., 2015; Tsai et al., 2021). However, these methods have limitations in providing detailed spatial information on the prevailing architecture and its continuity. In contrast, geophysical techniques play a crucial role in offering spatial insights into subsurface properties and processes (Crook et al., 2008). One great advantage of these techniques lies in their capability to provide spatially dense data over large areas, at a very limited cost, being totally non-invasive or minimally invasive. In this manner, geophysical methods can help establish a geometrical link between contamination distribution and site heterogeneity, especially concerning the presence of less permeable layers, as revealed by extensive surface geophysical measurements (e.g. Cassiani et al., 2014). Additionally, they establish a connection between contamination and specific geophysical signals, evident from cross-hole measurements (e.g. Arato et al., 2014; Revil et al., 2017). Methods such as 2D electrical resistivity profiling and vertical electrical sounding play a key role in mapping and characterizing high-resistivity structures indicative of oil plumes, while the need to validate geophysical results through soil sampling and analysis becomes evident (Raji et al., 2018). The consistency of electrical resistivity with borehole sampling results, where high resistivity corresponds to increased LNAPL concentration, has been observed (Xia et al., 2021). The combined application of geoelectrical and geochemical methods

effectively describes the distribution of underground contaminant plumes in aged pollution sites (Shao et al., 2019). These methods, collecting multiple data sets through time, allow for a quantitative assessment of aquifer vulnerability to surface pollutants (Deiana et al., 2007). Resistivity monitoring has been experimentally employed to investigate contaminant migration in heterogeneous soil layers under conditions of fluctuating water levels (Pan et al., 2021). The specific discipline of hydrogeophysics, in particular, establishes links between hydrologically relevant properties and measurable geophysical parameters. Time-lapse approaches have further enhanced hydrological investigation tools, revealing the sensitivity of some geophysical properties to biogeochemical transformations (Rubin and Hubbard, 2006; Vereecken et al., 2006; Binley et al., 2010; Binley et al., 2015). Hydrogeophysical tools can also be employed to depict the evolving situation resulting from the implementation of remediation strategies. For example, Mao et al. (2015) utilize time-lapse self-potential signals to monitor the remediation of a contaminant plume. In sandbox experiments, Mao et al. (2016) apply the direct current resistivity technique to image conductivity changes, enhancing hydrocarbon removal by a bioelectrochemical system (BES). Foam and reagent solutions injections in soil are tracked using visual observation and differential electric resistivity tomography (ERT) (Bouzid et al., 2021). In the treatment of ISCO with sodium permanganate, an electrically conductive oxidant, Harte et al. (2012) demonstrate its strong electrical signal for tracking injectate transport through time series geophysical surveys, including direct current (DC) resistivity and electromagnetic (EM) methods. Time-lapse two-dimensional bulk conductivity and induced polarization surveys conducted during a sand tank ISCO simulation allow remote monitoring of the fate and transport of ionic oxidants during the remediation of contaminants such as trichloroethene (TCE) (Hort et al., 2015). Xia et al. (2023) employ ERT for monitoring ISCO during the remediation process of diesel-contaminated soil. Differencing between pre-injection and post-injection ERT determines the distribution of the injected oxidant (Tildy et al., 2017). Cross-borehole and time-lapse resistivity models depict the spread of the oxidizing agent as highly conductive anomalies, confirmed by water conductivity measurements in boreholes (Bording et al., 2021). In some cases, although geophysical methods map the distribution of injected oxidants, the coupling of hydrochemical monitoring from downgradient wells and direct-push profiles does not yield sufficient data to quantify the distribution and flow behavior of the injected oxidant (Halihan et al., 2012; Tsai et al., 2021). Moreover, the imaging of the injectant spatial spreading, as captured through time-lapse monitoring, is rarely coupled with hydrochemical monitoring that jointly explains the physical processes occurring during in-situ remediation, the decontamination behavior, and the chemical transformations of pollutants during LNAPL ISCO.

1.4. Case study: enhancing LNAPL remediation and geoenvironmental understanding in a military airport site

In this context, an innovative technology that combines ISCO and enhanced desorption has been applied full scale at a site contaminated by petroleum hydrocarbons, in order to treat residual LNAPL and enhance the effectiveness of groundwater extraction and treatment systems. The study site is a military airport located in Sardinia, impacted by historical spills of approximately 50 m^3 of jet fuel, contaminating the groundwater in the tank farm area. Previous studies have identified, with high vertical resolution, the presence of contaminants, defined the volumes impacted by secondary sources of contamination, and unveiled the presence of residual free-phase/adsorbed hydrocarbons in the water table fluctuation zone. The conceptual site model (CSM) reveals that decades of P&T system activities have facilitated the smearing of the product near the hydraulic barrier wells (Ciampi et al., 2021, 2022; Flores-Orozco et al., 2021).

As part of the research presented in this paper, the performance of an enhanced remediation action, specifically targeting LNAPL and involving reagent injections into the subsurface to stimulate the desorption and oxidation of residual hydrocarbons, is monitored via a coupled geophysical-chemical monitoring approach to gain insights into the distribution of reagents in the subsurface and the effective reduction of pollutant concentrations. Geophysical monitoring, utilizing ERT, has the goal of revealing subsurface dynamics through variations in electrical conductivity during injection, extraction, and subsequent pumping activities. Hydrochemical sampling aims at unveiling the mechanisms of mobilization/dissolution of the residual fraction in space-time. The hydrogeophysical and data-driven framework explains the decontamination behavior on the basis of variations of electrical properties, providing considerable qualitative-quantitative insights into both the distribution of products in a highly heterogeneous medium, the extreme heterogeneity of contaminant degradation, as well as the hydraulic perturbations associated with the pumping operated by traditional physical extraction wells. The results of this research project thus enhance our understanding of decontamination processes, emphasizing the added value of a multi-source hydrogeophysical viewpoint in addressing the complexities of heterogeneous geological environments, and interpreting the spatial and temporal physio-chemical changes during the remediation process. The contribution of this research is twofold. On one hand, it significantly advances the overall understanding of the complex mechanisms involved in enhanced desorption and ISCO, offering comprehensive insights into both the spatial and temporal spreading of injectants and the physico-chemical transformation dynamics of pollutants during the remediation process. On the other hand, the paper showcases a sophisticated and pioneering approach to contaminant remediation, combining reagent injection, geophysical monitoring, and hydrochemical analysis. This advances our capacity to fine-tune and customize remediation strategies, particularly in heterogeneous environmental contexts, thus driving forward environmental remediation practices.

2. Materials and methods

2.1. Methodology for contaminant remediation: injection strategy, geophysical monitoring, and chemical analyses

The designed remediation strategy aimed at facilitating the mobilization of residual contaminants by introducing reagents through 14 specifically constructed wells, followed by the subsequent extraction of groundwater from the same injection stations. Fourteen drilling investigations were completed at the identified injection points to gather information on the local stratigraphy and to position the piezometer windows in relation to the saturated thickness of the aquifer. The injection operations were carried out in two distinct phases, initially within the internal area of the airbase tank farm (phase I) and subsequently at the site Southern boundary (phase II), that corresponds to the groundwater outflow boundary.

Geophysical monitoring through electrical resistivity tomography (ERT) was conducted before, during, and after the reagent injection along two lines, one located within the internal portion of the tank area (corresponding to the injection phase I) and the other at the site boundary (phase II) (Fig. 1a). The ERT lines were designed to highlight subsurface portions near the injection points used for reagent introduction. Phase I's AB line consisted of 48 electrodes, while phase II's CD line comprised 96 electrodes. In both cases, a 1 m electrode spacing was employed, adopting a dipole-dipole skip-4 (i.e. the dipole length is equal to 5 m, skipping 4 electrodes in between) acquisition scheme. Complete reciprocal acquisition, exchanging the potential with the current electrodes, was performed to estimate acquisition errors and eliminate anomalous elements before data inversion (Binley and Kemna, 2005; Cassiani et al., 2014). ERT data inversion was carried out using the Profiler-R2 program set provided by Lancaster University (http://www.es.lancs.ac.uk/people/amb/Freeware/R2/R2.htm), incorporated into the ResIPy package (Blanchy et al., 2020). The acquisition of ERT

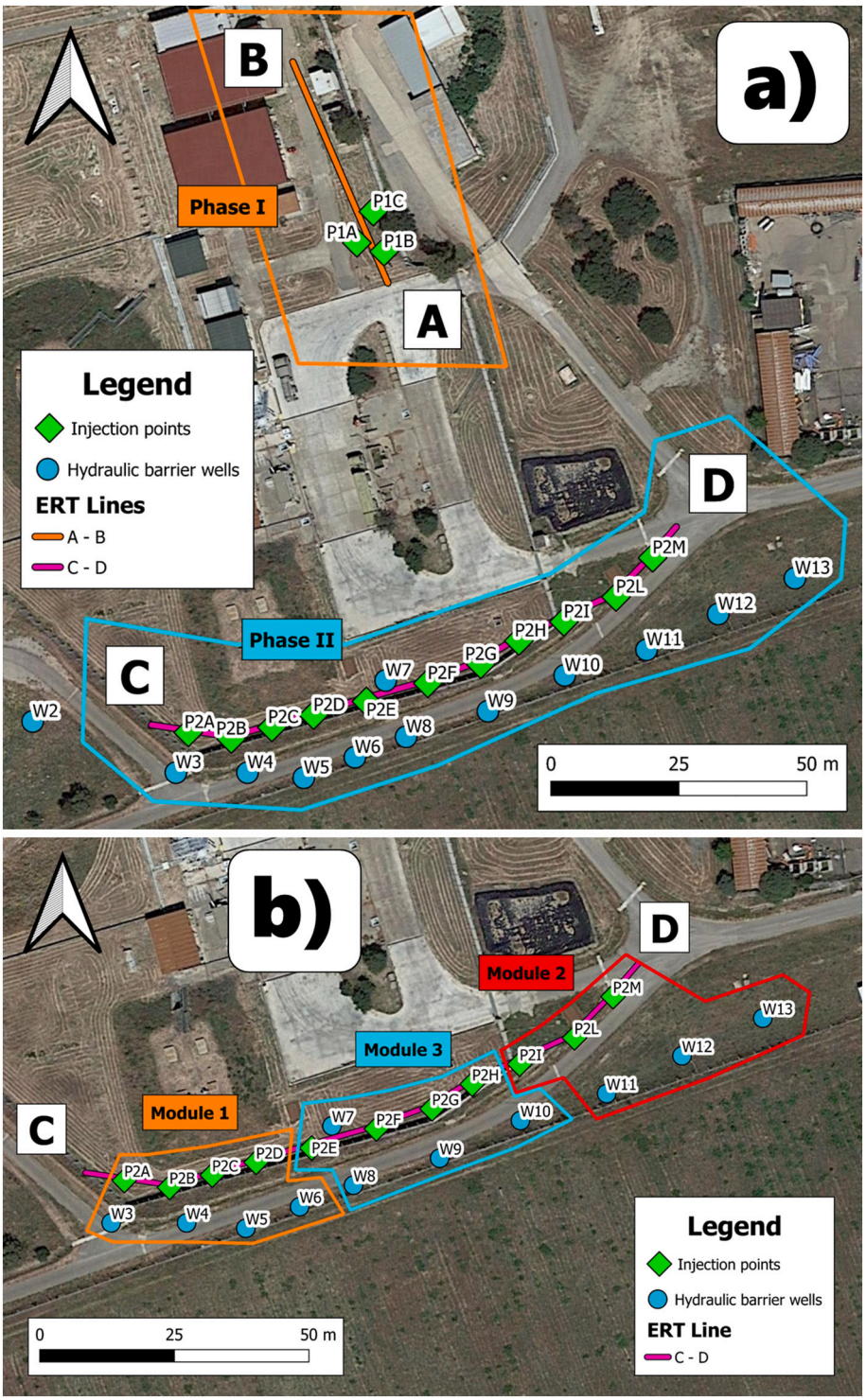

Fig. 1. Localization of the 14 reagent injection points, the AB line in the internal area of the tank farm (phase I), and the CD line near the site Southern boundary (phase II) (a). Schematic representation of the injection modules that make up the intervention front at the site boundary (phase II) (b). The maps illustrate the locations of the pumping wells that form the hydraulic barrier of the airbase (a, b).

profiles during different operational phases aimed at capturing variations in electrical conductivity over time as a consequence of reagent injection, providing insights into the distribution of products in a highly heterogeneous geological environment and hydraulic disturbances related to subsequent extraction at injection points and hydraulic barrier wells.

During phase I, injections were carried out at the piezometers located within the tank farm (P1A, P1B, P1C – see Fig. 1a), while maintaining the extraction operations from the hydraulic barrier wells at the site boundary. Phase I activities were completed in two days. In Phase II, reagent introduction activities sequentially shifted to three modules/segments of injection forming the intervention front at the site boundary (P2A, P2B, P2C, P2D, P2E, P2F, P2G, P2H, P2I, P2L, P2M) (Fig. 1b). Injection activities at the Southern site boundary extended over approximately 6 days. The hydraulic barrier wells downstream of each intervention module were temporarily shut down during the injection

operations in each segment, to be reactivated approximately 3 days after the completion of modular activities. The 11 wells comprising the hydraulic barrier collectively pumped approximately 3.3 m^3/h of groundwater. The authors demonstrated how hydraulic containment altered the natural groundwater flow, resulting in local depressions of the piezometric surface of about 3 m at the site boundary (Ciampi et al., 2021, 2022; Flores-Orozco et al., 2021). Temporarily shutting down the wells at the site boundary in a modular fashion aimed at minimizing the hydraulic disturbances associated with extraction operations in the in situ treatment zones and at limiting the drawdown of injected reagents from the nearby barrier wells. In the treatment zones, injections were performed under undisturbed laminar flow conditions, with a predominant NE-SW groundwater flow direction and a flow velocity estimated at around 30 m/year (Ciampi et al., 2022). This strategy aimed at effectively dispersing injected products within the influence areas of injection points, enhancing chemical delivery through advective and diffusive transport to targeted zones, extending contact time between the contaminated aquifer and reagents, and ultimately promoting desorption and oxidation processes of the residual fraction heterogeneously redistributed in the complex local geological architecture. Reactivating the extraction wells after the modular treatment aimed at ensuring the containment of mobilized and dissolved hydrocarbon fractions within the site (Table 1).

The injections utilized a mixture of two components: a desorbing agent (PetroCleanze®) and an oxidizing agent (RegenOx®). Both products are commercially distributed by Regenesis® (Regenesis, 2023). At each intervention point, PetroCleanze® was applied first, followed by rinsing each injection point with approximately 100 L of water. After injecting the first component in each module, there was a pause period of about 1 day to favor the prolonged contact of the desorbing solution with the residual contaminant. Then, the RegenOx® solution was added, followed by rinsing the injection sites with an additional 100 L of water per point. The combined application of these chemicals aimed at increasing the desorption rate of hydrocarbons sorbed to the saturated soil, stimulate the in-situ chemical oxidation of contaminants, and enhance their removal through physical recovery or pumping at the injection points (Ciampi et al., 2021). Table 2 provides the volumetric breakdown of both the injected and removed product volumes at each injection point, as well as the injection and pumping rates for each of the two components that make up the mixture. The volume pumped following the injection activities of phases I and II amounts to approximately twice the volume of reagent injected in each module.

The sampling and chemical analysis of groundwater were conducted to verify the effective mobilization and dissolution of residual hydrocarbon components induced by the introduction of the reagents. In total, four analysis campaigns were carried out with a monthly sampling frequency, for each injection point. Analytical determination of dissolved concentrations in groundwater was coupled with the speciation analysis of different hydrocarbon fractions to gain insights into the chemical-physical mechanisms of contaminant removal and in situ degradation. These analyses were replicated at point W4, corresponding to a hydraulic barrier well, reactivated after the phase II injection activities. Chemical analyses on a barrier well aimed at unveiling the influence of hydraulic disturbances induced by physical pumping on the physico-chemical degradation processes of contaminants linked to reagent injection.

Table 1
Schematic representation of the sequence of injection activities in the three intervention modules at the site boundary (phase II), indicating both the injection points and the hydraulic barrier wells present in each segment.

Intervention module at the hydraulic barrier along the Southern site boundary	Injection points for each intervention module	Hydraulic barrier wells within the intervention module
1	P2A	W3
	P2B	W4
	P2C	W5
	P2D	W6
2	P2I	W11
	P2L	W12
	P2M	W13
3	P2E	W7
	P2F	W8
	P2G	W9
	P2H	W10

3. Results

3.1. Geological stratigraphy and hydrogeological characteristics of subsurface zones

The stratigraphy observed in the 14 boreholes drilled for the installation of injection points reflects the site geology as previously reconstructed and presented in earlier studies (Ciampi et al., 2021, 2022; Flores-Orozco et al., 2021). The site geology along the AB and CD sections covering the subsurface portions near the injection points is depicted in Fig. 2 (obtained by interpolation of the many existing drilling points) and can be summarized as follows from top to bottom:

- Filling and anthropogenic materials with an average thickness of 0.2 m.
- A layer consisting of gravels and sands with the presence of fine particles, with a variable thickness ranging from 3 to 5.5 m.
- An intercalation of hazel-colored sandy-gravel clays with spatial non-continuity, reaching a maximum thickness of 1.3 m.
- Gravel and sand in a silt-clay matrix at depths ranging from 4.6 to 6.8 m.
- A deposit of clays and silty clays down to a depth of 12 m from the ground level (Fig. 2).

The alluvial deposits in the shallowest 7 m host groundwater circulation, while the underlying silty clays act as an aquiclude. The average hydraulic conductivity for gravels and silty sands (9.3×10^{-5} m/s), sandy-gravelly clays (4.2×10^{-9} m/s), and gravels and sands in a silty-clayey matrix (8.6×10^{-7} m/s) has been derived from earlier studies performing grain size analyses on samples collected from the airbase (Flores-Orozco et al., 2021). The groundwater table lies at an average depth of 3.2 m.

3.2. Thorough geoelectric assessment of subsurface dynamics: insights from multi-temporal ERT profiles

The acquisition of resistivity profiles before, during, and after the injection of reagents in the internal area during phase I, allows us to picture the changes in electrical conductivity of the subsoil as a consequence of the presence of reactive substances and their interaction with both the natural system and the contaminants present in the porous medium. This entails, also, the identification of preferential pathways in the shallow subsoil that convey the reagents, and thus enhance in one sense, and hinders in another sense, the effectiveness of the remediation strategy.

The ERT background of profile AB outlines the shape of clayey and silty clayey formations bounding the alluvial aquifer, characterized by an electrical resistivity of less than approximately 60 Ω·m. The sediments encountered in the shallowest 7 m result in a pronounced variation in electrical properties also in the horizontal direction, with an electrical resistivity ranging from 60 to 300 Ω·m (Fig. 3a). Fig. 3b illustrates the variation (% change) in electrical properties after the injection of PetroCleanze. The injection of desorbent induces a slight decrease in resistivity (increase in electrical conductivity), locally around 10 %, in the saturated portions near the injection points. The increase in electrical conductivity (decrease in resistivity) is more pronounced in Fig. 3c, depicting the resistivity variation scenario following

Table 2
Comparison of flow rates and volumes of injected and extracted products at the 14 injection points, summarizing the volumes of product injected in the two phases in the intervention modules.

Injection point	Desorbent injection rate (L/min)	Injected desorbent volume (L)	Oxidant injection rate (L/min)	Injected oxidant volume (L)	Volume of injected products (L)	Pumping rate (L/min)	Pumped mixture volume (m^3)
P1A	10	1050	25	1050	6300	13	12
P1B	20	1050	14	1050			
P1C	20	1050	20	1050			
P2A	10	1450	23	1450	9200	14	18
P2B	21	1050	23	1050			
P2C	23	1050	23	1050			
P2D	24	1050	23	1050			
P2I	23	1050	22	1050	6300	10	12
P2L	23	1050	22	1050			
P2M	23	1050	22	1050			
P2E	23	1050	23	1050	8400	20	20
P2F	23	1050	22	1050			
P2G	23	1050	23	1050			
P2H	24	1050	23	1050			

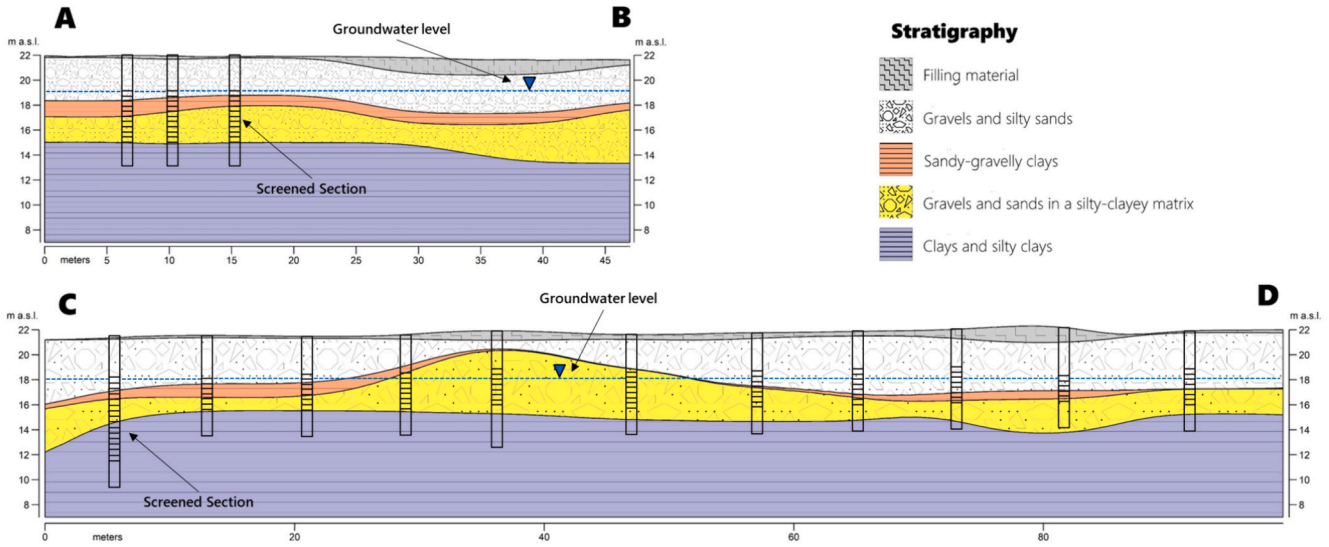

Fig. 2. Geological sections created along the ERT profiles AB and CD, covering the subsurface portions affected by the introduction of reagents through the injection points.

the injection of RegenOx. The distribution of oxidant in the aquifer is evidenced by a 30 % increase in electrical conductivity around the screened sections of the injection wells. Fig. 3d, acquired after the pumping activities, reveals a general decrease in electrical conductivity along the profile and the contraction of low resistivity plume, due to the extraction of injected products. Some surface clouds with a marked decrease in resistivity compared to the background, ranging from 20 to 30 %, appear in the middle portions of Fig. 3c and d. These represent zones characterized by a decrease in electrical conductivity due to the upwelling of injected products along preferential fluid transport conduits. This interpretation is supported by the time-lapse geoelectric surveys and is validated by field activities, where the emergence of products near the middle portion of the ERT section became evident. Local increases in resistivity, observed both at the surface and at depths ranging from 3 to 7 m, could spatially delineate the mobilization processes of residual contaminants adsorbed to the geological matrix. Enclosed anomalies with a decrease in electrical conductivity of 5–10 % are observed immediately upon desorbent injection (refer to Fig. 3a). The increase in resistivity is mitigated by the injection of electrically conductive oxidant (see Fig. 3b). During the extraction of injected solutions (see Fig. 3c), well-defined increases in resistivity of 10–15 % compared to the background suggest and paint in two dimensions the progression of desorption processes of aged contaminants in specific areas of an extremely heterogeneous domain.

The interpretation of ERT profiles acquired during the execution of activities of Phase II refines the geological model and reflects the sequence of injection and extraction activities at the injection stations and wells of the hydraulic barrier. The ERT background outlines an anomaly with high resistivity, ranging from approximately 200 to 700 Ω·m, between the progressive distances of 58 m and 68 m and at a depth of about 7 to 14 m below ground level. This potentially represents a portion of the aquifer composed of coarse deposits, thus having a higher permeability (Fig. 4a). This zone corresponds to the clays and silty clays in the geological section CD of Fig. 2, as Fig. 2 is constructed by interpolation of local borehole stratigraphies, this procedure evidently fails to discriminate this subsurface portion with high hydraulic conductivity. Fig. 4b depicts the resistivity variation compared to the background along profile CD, following the introduction of both reagents, pull activities at the injection stations located to the west of the profile (P2A, P2B, P2C, P2D), and the activation of wells in the hydraulic barrier at module 1 (W3, W4, W5, W6). Bands with a 20 % decrease in resistivity, locally reaching a 60 % increase in electrical conductivity compared to the background, illustrate the heterogeneous diffusion of products in both saturated and unsaturated domains, depicting the distribution of reagents in two dimensions. The distribution of desorbent and oxidant is evident primarily in the area of high hydraulic conductivity depicted in

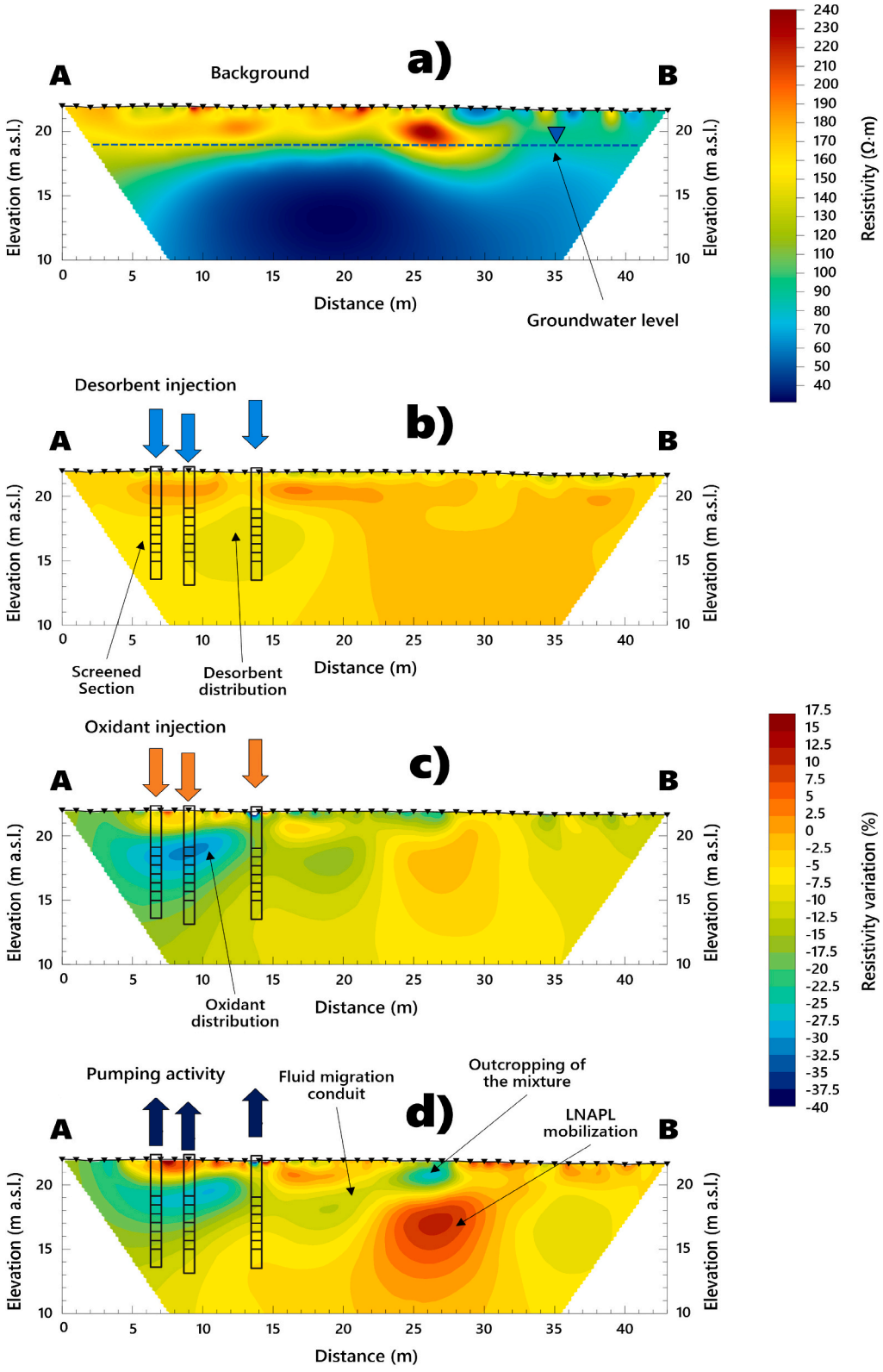

Fig. 3. 2D sections showing the percentage variation in resistivity compared to the background (a) recorded in Phase I along the AB profile: after the injection of desorbent (b), following the addition of oxidant (c), and following the physical extraction by pumping (d). The image also shows the location and position of both the injection point windows and the water table.

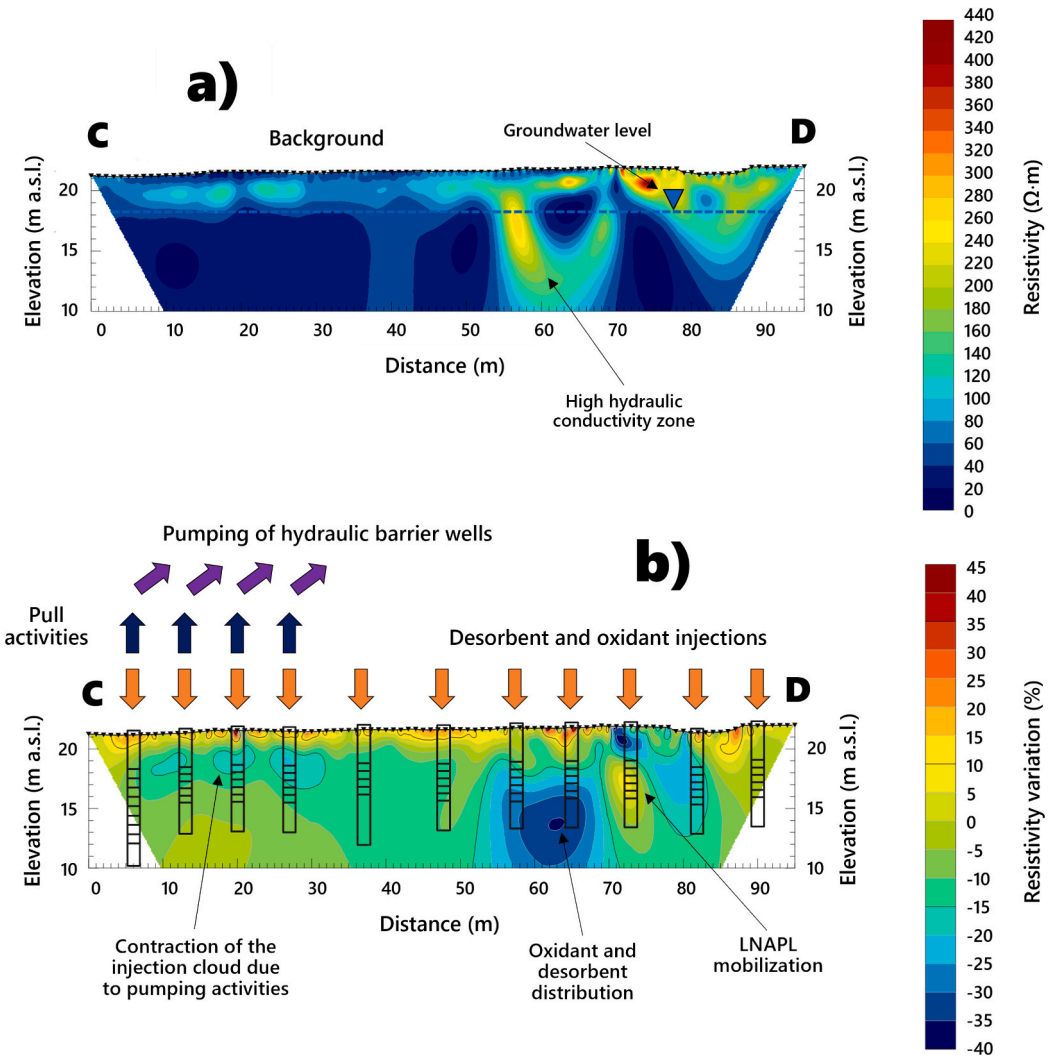

Fig. 4. Two-dimensional section CD depicting the percentage variation in resistivity compared to the background acquired in Phase II after conducting injections and pull activities at the site boundary and following the reactivation of wells in the hydraulic barrier of module 1. The image illustrates the location and position of the injection point windows along with the groundwater table elevation.

Fig. 4a. In the western sector of the Fig. 4b profile, more modest increases in electrical conductivity and the contraction of the low resistivity clouds (with a 20 % resistivity decrease compared to background) suggest the potential contribution of both pull activities at injection stations P2A, P2B, P2C, P2D, and pumping operations at wells of the hydraulic barrier to the physical extraction of injected solutions and fractions of mobilized and dissolved contaminants in groundwater. Furthermore, increases in resistivity ranging from 10 % to locally 40 % emerge both in surface horizons and in bands at depths ranging from 3 to 6.5 m (Fig. 4b). These anomalies reflect the findings acquired in Phase I and highlight the subsurface areas where desorption of sorbed-phase or smeared hydrocarbons occur. Moreover, by comparing Fig. 4a and b, the decrease in electrical conductivity appears primarily associated with fine-grained deposits with low electrical resistivity, well-documented in literature for their capacity to adsorb contaminants in residual phase. For instance, such variation in resistivity trend is distinctly evident at depths around 4 m along the progressive distance of 73 m.

Geoelectric prospecting in near real-time during different stages of planned activities is thus capable of sensing the effects of injections, as the introduction of reagents into the aquifer results in variations in the electrical properties of the subsurface (electrical conductivity). Some 2D images represent changes in the resistivity of materials both vertically and horizontally, detailing with high resolution the anisotropy of the subsurface and the dispersion modes of both the desorbent and oxidant in the aquifer. The multi-temporal ERT profiles potentially also capture the variation in electrical conductivity due to the dynamic sequence of injection operations and hydraulic mechanisms induced by physical extraction activities on both groundwater, injected solutions, mobilized, and dissolved pollutants.

3.3. Hydrochemical transformations and mobilization processes in groundwater contamination remediation

The hydrochemical monitoring of groundwater before and after reagent injection highlights an effective mobilization process of residual hydrocarbon fractions at the injection wells. The concentrations of dissolved total petroleum hydrocarbons (TPH) in groundwater at the 14 application points of the desorbent and oxidant progressively increased from an average value of 232 μg/L, measured before the injections, to 542 μg/L, 925 μg/L, and 1004 μg/L in the monitoring conducted one month, two months, and three months after the introduction of the reagents, respectively. The mobilization/dissolution rates of the residual fraction in space-time appear to be extremely heterogeneous within the monitored monitoring interval (Fig. 5).

The speciation analysis of total hydrocarbons detected at injection points reveals decontamination dynamics and the mechanisms of

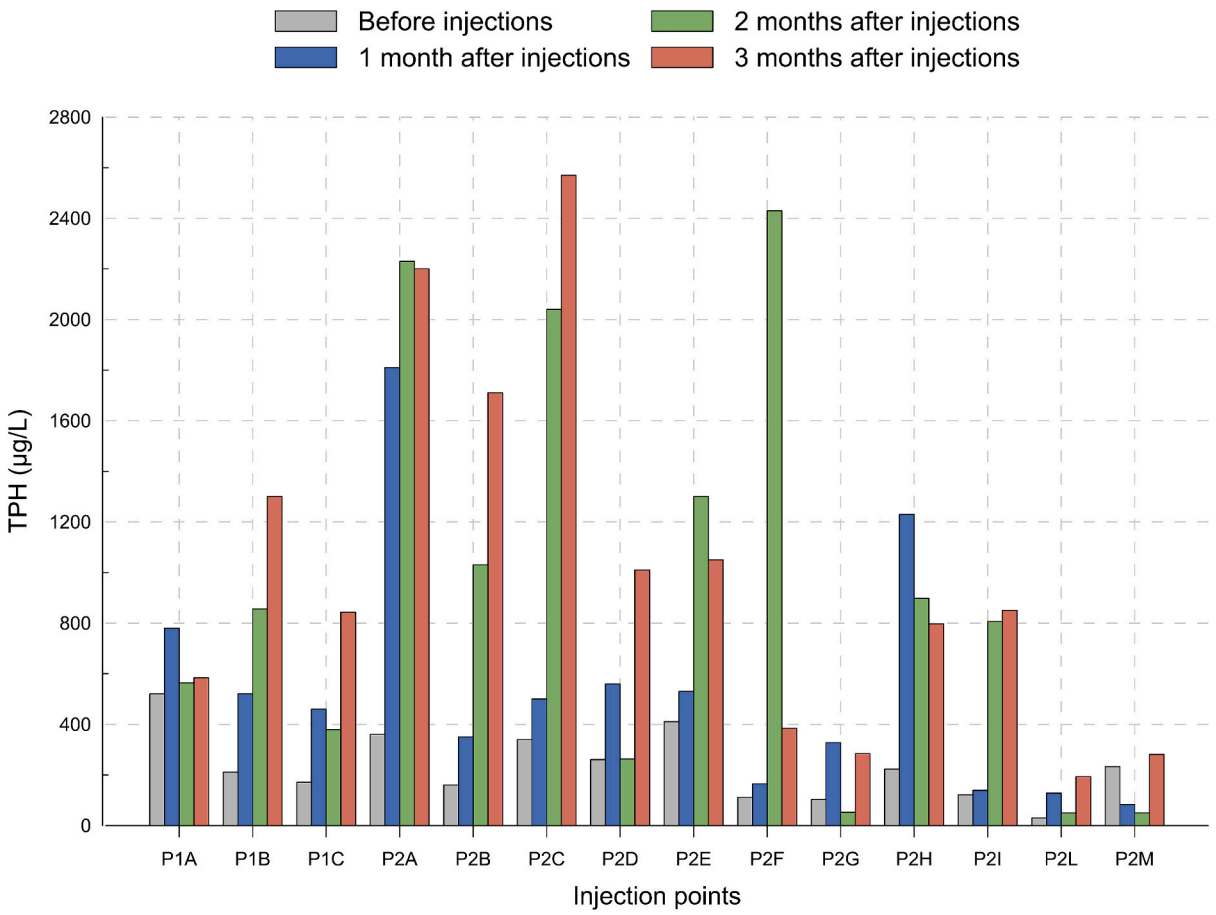

Fig. 5. Concentrations of total petroleum hydrocarbons (TPH) detected at the 14 injection points along line CD, before and in the three months following the injection of reagents.

physical desorption and chemical oxidation over space and time. Analyses carried out one month after the injection of reagents unveil an escalation in hydrocarbon concentrations within the aquifer (Fig. 6b), contrasting with the levels observed in the previous sampling (Fig. 6a). This increase is likely associated with the physical desorption of heavier fractions followed by their dissolution into the groundwater. The impact of the oxidant emerges two months after the introduction of reagents, entwined with the dissolution of lighter hydrocarbon fractions (Fig. 6c). Three months after the completion of remediation activities, heavier fractions predominate, revealing a reversal in the hydrocarbon fractionation ratio compared to the previous sampling (Fig. 6d). Extended purging activities yield measurements of higher molecular weight fractions, reflecting the draw of desorbed fractions from more distant portions towards the injection stations.

These findings suggest the potential influence of push and pull activities, the sequence of product injection, and pumping operations conducted by the wells of the hydraulic barrier at the site's boundary on the evolving dynamics of fractionation. Confirmation of these statements is evident in the temporal evolution of fractionation at W4, mirroring that observed at the injection sites and vividly portraying the reagent's journey through time. Post-injection, the effects of desorption processes shift towards the W4. In the two months following the injections, along with an increase in TPH concentrations, a rise in the proportion of heavier fractions compared to counterparts with lower molecular weight is registered. This phenomenon reflects the extraction and sampling of groundwater, where the mobilization of higher molecular weight fractions has been facilitated by the desorbent. The effects of introducing the oxidizer steal the show at the hydraulic barrier well three months after the reagent application activities and exhibit the predominance of lighter fractions compared to the preceding month (Fig. 7).

The canvas of chemical analyses intricately depicts the unfolding processes of desorption and oxidation across space and time, asserting that these chemicals play a pivotal role as enhancers for the dynamic P&T system.

4. Discussions

In line with Pac et al.'s (2019) findings, collaborative datasets provide multiple layers of supporting evidence facilitating a more targeted approach to the design and implementation of ISCO. A configuration that embraces a combination of short-screened injection intervals and a greater number of injection locations translates into smaller radii of influence (ROI) per injection station, thereby minimizing the risk of delivering excessive oxidant volumes into preferential pathways (Huling et al., 2017). The distinctive shape of electrical resistivity anomalies becomes apparent immediately following the injection of each product, closely mirroring the lithological framework (Tildy et al., 2017). Low-resistivity plumes paint a vivid picture of the migration pathways of the desorbent and oxidant in both space and time under field conditions, aligning with observations in experimental settings and affirming the potential of time-lapse ERT images in capturing the delivery and fate of reagents in ISCO remediation (Bording et al., 2021; Hort et al., 2015). While the variation and decrease in resistivity are primarily influenced by the migration of the injected plumes, one must consider the contribution related to the consumption of contaminants and the generation of degradation products, which may contribute to the decline in electrical conductivity (Xia et al., 2023). Localized decreases in electrical

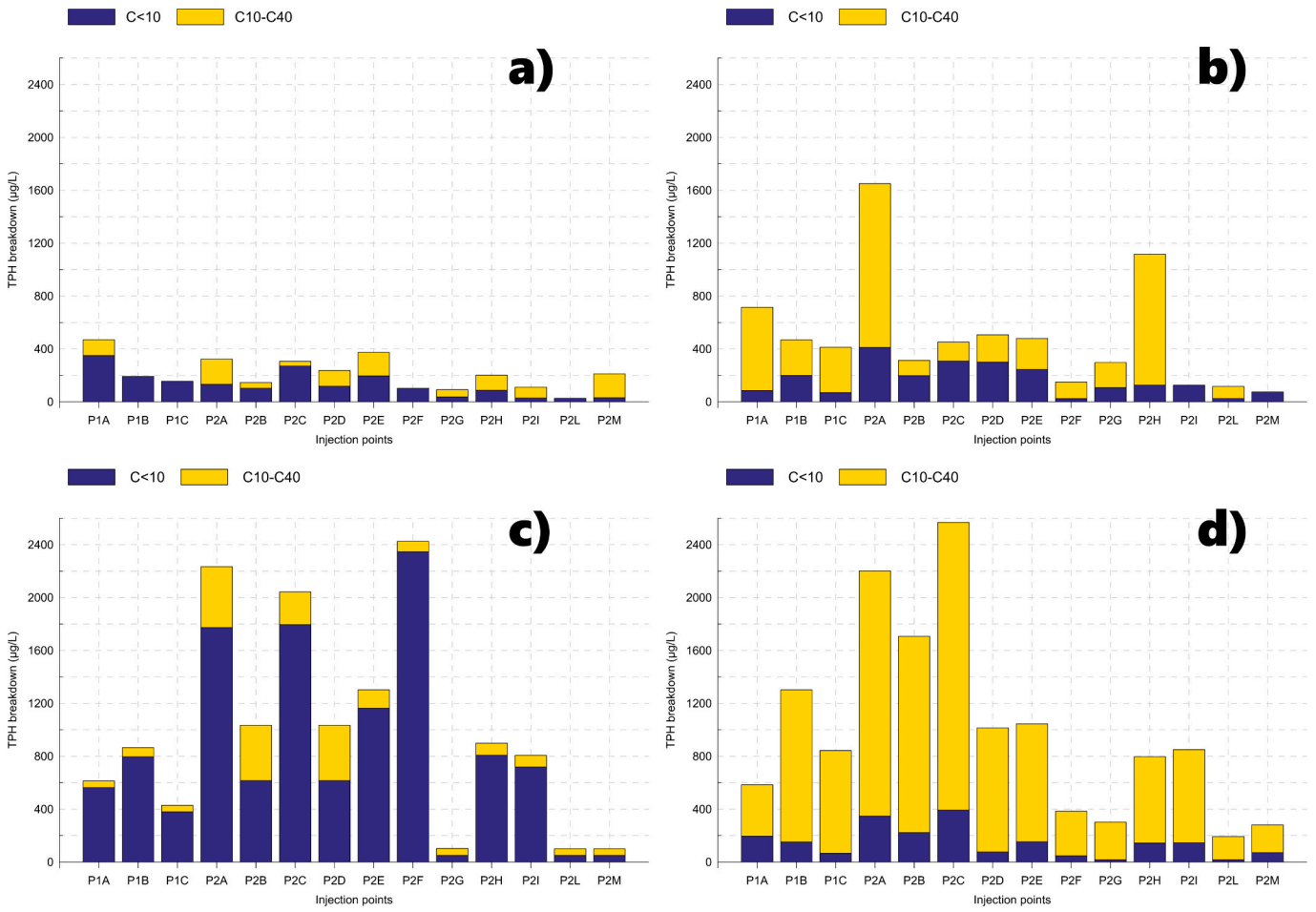

Fig. 6. Concentrations of light hydrocarbon fractions (C < 10) and heavy fractions (C10-C40) measured in the 14 reagent introduction wells along line CD, before (a), one (b), two (c), and three (d) months after the injection activities.

conductivity may be associated with the mobilization of adsorbed products in the residual phase due to the action of the desorbent. Increases in resistivity during injection activities are observed at fine geological horizons corresponding to low-resistivity anomalies collected during characterization, known for being notorious sources of residual LNAPL accumulation (Cavanagh et al., 2014). Information gathered during the pilot test of the intervention had already highlighted localized increases in resistivity due to the desorption of residual product adsorbed to the solid matrix (Ciampi et al., 2021). This trend has been confirmed by the full-scale intervention and the stepwise refinement of the CSM. The aquifer's spatially diverse response in terms of mobilized concentrations mirrors the hydrogeochemical and physical complexity of the contamination scenario. The authors' reconstructed conceptual framework of the site has unveiled the adsorption of LNAPLs at local low-permeability levels and the spatially heterogeneous redistribution of the residual phase due to seasonal oscillations of the groundwater table and the development of the cone of depression induced by on-site physical pumping activities (Ciampi et al., 2022). The application of the desorbent and oxidizer has selectively impacted and mobilized residual and aged fractions of pollutants with limited mobility/solubility adsorbed to the solid matrix, persisting despite conventional physical groundwater extraction activities on-site. The introduced reagents favor and enhance the removal of contaminants through pump-and-treat (P&T) at a site characterized by long-term contamination (Ciampi et al., 2021). The results suggest the occurrence of desorption and oxidation processes even after pumping activities (Besha et al., 2018; Sharma et al., 2020). The increase in TPH concentrations in the three months following the introduction of reagents suggests an extended contact with trapped, immobile, or inaccessible compounds—materials located in areas that are inaccessible to liquid-based reagents, including no-flow zones, dead-end pores, and immobilized material. These materials, evidently present in significant quantities, locally necessitate a further injection application (Pac et al., 2019). In contrast to the findings of Halihan et al. (2012) and Tsai et al. (2021), groundwater sampling at the hydraulic barrier well monitors fluid dynamics and proves skillful in tracing the reactive flow behavior of reagents and the desorption and oxidation processes over space and time, validating the chemical enhancement of P&T.

The hydrogeophysical and data-driven perspective effectively distinguishes geophysical evidence and the variation of electrical properties over space-time, leveraging lithologic characteristics and contamination effects. Although the interpretation of ERT findings is influenced by both geological characteristics and the effects of contamination and reagent injection, several authors have demonstrated how time-lapse electrical conductivity changes dynamically monitor the ISCO in-situ remediation process, especially the spreading of the oxidants plume (Arato et al., 2014; Hort et al., 2015; Pac et al., 2019; Xia et al., 2023). On the other hand, it is difficult to directly distinguish the effects of the oxidant plume, the presence of residual oxidant, LNAPL distribution in residual and dissolved phases, adsorption/desorption behavior, contaminant consumption, soil characteristics, pollutant concentrations, generation, and migration of degradation products on resistivity changes. For these reasons, a comprehensive analysis combined with chemical sampling data is required to reduce uncertainties associated with subsurface interpretation. This approach yields substantial qualitative and quantitative insights into the distribution of

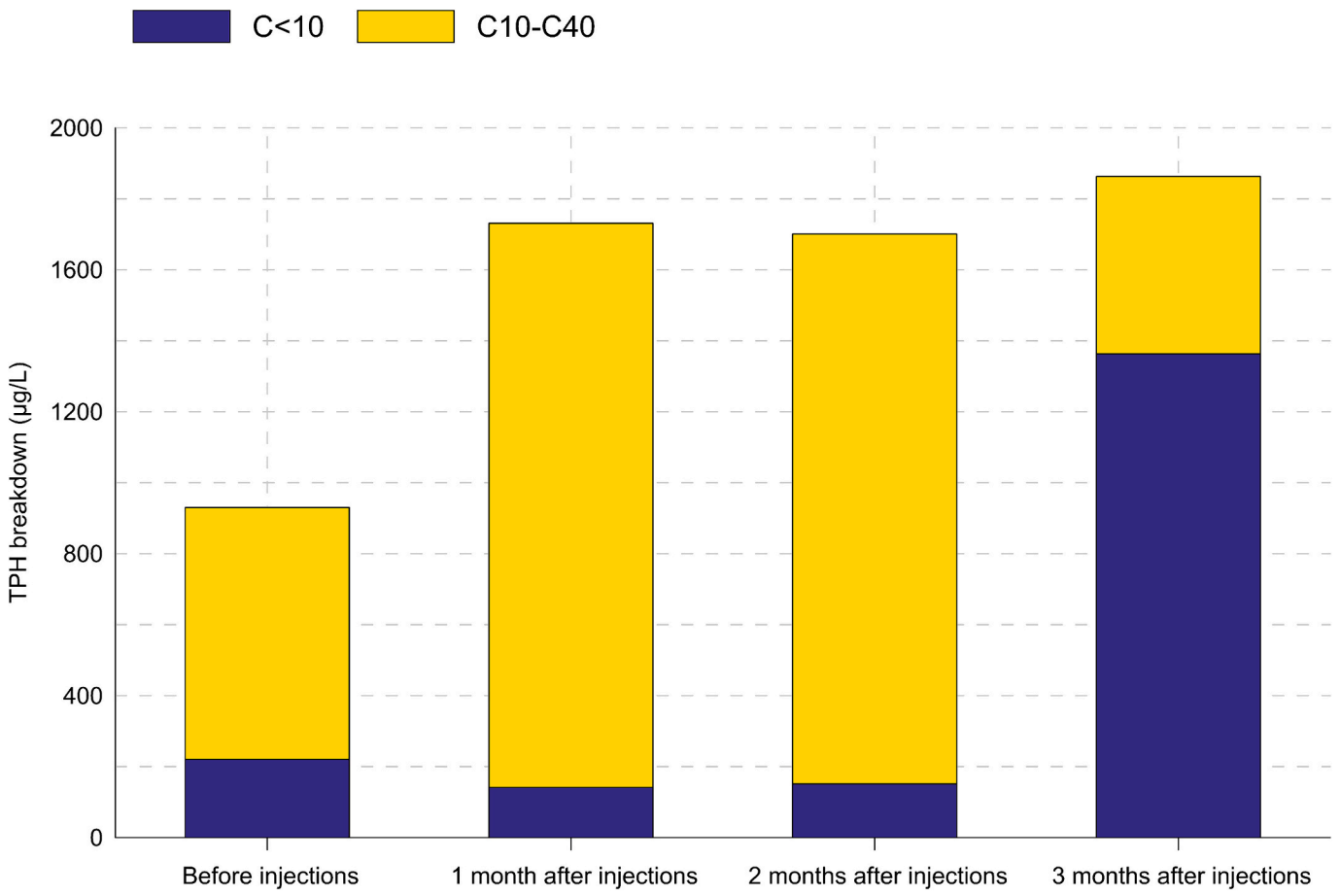

Fig. 7. Concentrations of light hydrocarbon fractions (C < 10) and heavy fractions (C10-C40) measured in the hydraulic barrier well W4 before and in the three months following the injection activities of the desorbent and oxidizer.

products within a highly heterogeneous medium, the mobilization/dissolution of the residual fraction in a space-time that is extremely diverse, and the hydraulic perturbations associated with pumping operations carried out by traditional physical extraction wells, whose performance is enhanced by the coupling of improved desorption and ISCO. The findings vividly portray the evolving geophysical signature of decontamination dynamics and mechanisms, shedding light on the spatial and temporal physio-chemical behaviors and changes during the remediation process. This nuanced understanding contributes significantly to the overall comprehension of the intricate processes involved in the enhanced desorption and ISCO strategy, enhancing our ability to optimize and tailor remediation efforts in heterogeneous environmental settings.

5. Conclusions

The remediation strategy presented in the text is a meticulously designed plan involving the injection of reagents through specifically constructed wells to mobilize and extract residual contaminants. The injection activities involve a mixture of a desorbing agent (PetroCleanze®) and an oxidizing agent (RegenOx®), showcasing an innovative approach to enhance the desorption of hydrocarbons and stimulate in-situ chemical oxidation of contaminants. The integration of geophysical monitoring via electrical resistivity tomography (ERT) and hydrochemical data allows for a data-driven understanding of the in-situ chemical oxidation (ISCO) remediation approach. The use of electrical resistivity profiles before, during, and after injection provides real-time insights into the subsurface dynamics, illustrating the pathways of reagent migration, delineating the mobilization of pollutants in space-time, and the impact on electrical conductivity. Two-dimensional sections effectively visualize changes in resistivity, offering a high-resolution understanding of the anisotropy, dispersion modes of desorbent and oxidant in the aquifer, mobilization of sorbed-phase or smeared contaminants, and pumping effects on injected solutions. The hydrochemical monitoring reveals effective mobilization processes, with concentrations of total petroleum hydrocarbons (TPH) increasing over time after reagent injection. Speciation analysis of hydrocarbons provides detailed insights into the dynamic processes of desorption and oxidation, demonstrating the effectiveness of the remediation strategy. The nuanced understanding of the contamination scenario, including adsorption of LNAPLs at low-permeability levels and spatially heterogeneous redistribution, highlights the complexity of the subsurface environment. The overlap of evidence derived from hydrogeophysical and chemical findings captures the transformations of pollutants following the sequence of product injection and push-and-pull activities, documenting the removal of mobilized contaminants through hydraulic barrier wells. The results contribute significantly to the overall comprehension of the intricate processes involved in enhanced desorption and ISCO, providing holistic insights into spatial and temporal physio-chemical behaviors during the remediation process. This nuanced understanding enhances our ability to optimize and tailor remediation efforts, particularly in heterogeneous environmental settings. In conclusion, the presented text showcases a sophisticated and innovative approach to contaminant remediation, combining geophysical monitoring, reagent injection, and hydrochemical analysis. The integration of various data sources provides a comprehensive understanding of the remediation process, contributing to the advancement of environmental remediation practices.

CRediT authorship contribution statement

Paolo Ciampi: Writing – original draft, Software, Methodology, Conceptualization. **Giorgio Cassiani:** Writing – review & editing, Supervision, Methodology, Investigation, Formal analysis, Data curation. **Gian Piero Deidda:** Writing – review & editing, Investigation, Data curation. **Carlo Esposito:** Visualization, Supervision. **Paolo Rizzetto:** Visualization, Supervision. **Andrea Pizzi:** Visualization, Supervision. **Marco Petrangeli Papini:** Validation, Supervision, Project administration, Methodology.

Declaration of competing interest

The authors declare that they have no known competing financial interests or personal relationships that could have appeared to influence the work reported in this paper.

Data availability

Data will be made available on request.

Acknowledgements

We extend our sincere gratitude to Paola Goria and Marcello Carboni from Regenesis for their invaluable technical assistance and collaboration throughout the planning, support, and implementation stages of the coupled injection of desorbent (PetroCleanze®) and oxidant (RegenOx®).

References

Algreen, M., Kalisz, M., Stalder, M., Martac, E., Krupanek, J., Trapp, S., Bartke, S., 2015. Using pre-screening methods for an effective and reliable site characterization at megasites. Environ. Sci. Pollut. Res. 22, 14673–14686. https://doi.org/10.1007/s11356-015-4649-6.

Arato, A., Wehrer, M., Biró, B., Godio, A., 2014. Integration of geophysical, geochemical and microbiological data for a comprehensive small-scale characterizationof an aged LNAPL-contaminated site. Environ. Sci. Pollut. Res. 21, 8948–8963. https://doi.org/10.1007/s11356-013-2171-2.

Barbati, B., Lorini, L., Amanat, N., Bellagamba, M., Galantini, L., Petrangeli Papini, M., 2023. Enhanced solubilization of strongly adsorbed organic pollutants using synthetic and natural surfactants in soil flushing: column experiment simulation. J. Environ. Chem. Eng. 11 (5), 110758 https://doi.org/10.1016/j.jece.2023.110758.

Besha, A.T., Bekele, D.N., Naidu, R., Chadalavada, S., 2018. Recent advances in surfactant-enhanced in-situ chemical oxidation for the remediation of non-aqueous phase liquid contaminated soils and aquifers. Environ. Technol. Innov. 9, 303–322. https://doi.org/10.1016/j.eti.2017.08.004.

Binley, A., Kemna, A., 2005. DC resistivity and induced polarization methods. In: Rubin, Y., Hubbard, S.S. (Eds.), Hydrogeophysics. Water Science and Technology Library, vol 50. Springer, Dordrecht, pp. 129–156. https://doi.org/10.1007/1-4020-3102-5_5.

Binley, A., Cassiani, G., Deiana, R., 2010. Hydrogeophysics – opportunities and challenges. Boll. Geofis. Teor. Appl. 51 (4), 267–284.

Binley, A., Hubbard, S.S., Huisman, J.A., Revil, A., Robinson, D.A., Singha, K., Slater, L. D., 2015. The emergence of hydrogeophysics for improved understanding of subsurface processes over multiple scales. Water Resour. Res. 51, 3837–3866. https://doi.org/10.1002/2015WR017016.

Blanchy, G., Saneiyan, S., Boyd, J., McLachlan, P., Binley, A., 2020. ResIPy, an intuitive open source software for complex geoelectrical inversion/modeling. Comput. Geosci. 137, 104423. https://doi.org/10.1016/j.cageo.2020.104423.

Bording, T., Kühl, A.K., Fiandaca, G., Christensen, J.F., Christiansen, A.V., Auken, E., 2021. Cross-borehole geoelectrical time-lapse monitoring of in situ chemical oxidation and permeability estimation through induced polarization. Near Surf. Geophys. 19 (1), 43–58. https://doi.org/10.1002/nsg.12131.

Bouzid, I., Herrera, D.P., Dierick, M., Pechaud, Y., Langlois, V., Klein, P.Y., Albaric, J., Fatin-Rouge, N., 2021. A new foam-based method for the (bio) degradation of hydrocarbons in contaminated vadose zone. J. Hazard. Mater. 401, 123420 https://doi.org/10.1016/j.jhazmat.2020.123420.

Brusseau, M.L., Guo, Z., 2014. Assessing contaminant-removal conditions and plume persistence through analysis of data from long-term pump-and-treat operations. J. Contam. Hydrol. 164, 16–24. https://doi.org/10.1016/j. jconhyd.2014.05.004.

Cassiani, G., Binley, A., Kemna, A., Wehrer, M., Flores-Orozco, A., Deiana, R., Boaga, J., Rossi, M., Dietrich, P., Werban, U., Zschornack, L., Godio, A., Jafargandomi, A., Deidda, G.P., 2014. Noninvasive characterization of the Trecate (Italy) crude-oil contaminated site: links between contamination and geophysical signals. Environ. Sci. Pollut. Res. 21, 8914–8931. https://doi.org/10.1007/s11356-014-2494-7.

Cavanagh, B.A., Johnson, P.C., Daniels, E.J., 2014. Reduction of diffusive contaminant emissions from a dissolved source in a lower permeability layer by sodium persulfate treatment. Environ. Sci. Technol. 48, 14582–14589. https://doi.org/10.1021/es5040443.

Cavelan, A., Golfier, F., Colombano, S., Davarzani, H., Deparis, J., Faure, P., 2022. A critical review of the influence of groundwater level fluctuations and temperature on LNAPL contaminations in the context of climate change. Sci. Total Environ. https://doi.org/10.1016/j.scitotenv.2021.150412.

Ciampi, P., Esposito, C., Cassiani, G., Deidda, G.P., Rizzetto, P., Petrangeli Papini, M., 2021. A field-scale remediation of residual light non-aqueous phase liquid (LNAPL): chemical enhancers for pump and treat. Environ. Sci. Pollut. Res. 28, 35286–35296. https://doi.org/10.1007/s11356-021-14558-2.

Ciampi, P., Esposito, C., Cassiani, G., Deidda, G.P., Flores-Orozco, A., Rizzetto, P., Chiappa, A., Bernabei, M., Gardon, A., Petrangeli Papini, M., 2022. Contamination presence and dynamics at a polluted site: spatial analysis of integrated data and joint conceptual modeling approach. J. Contam. Hydrol. 248, 104026 https://doi.org/10.1016/j.jconhyd.2022.104026.

Ciampi, P., Esposito, C., Bartsch, E., Alesi, E.J., Petrangeli Papini, M., 2023. Pump-and-treat (P&T) vs groundwater circulation wells (GCW): which approach delivers more sustainable and effective groundwater remediation? Environ. Res. 234, 116538 https://doi.org/10.1016/j.envres.2023.116538.

Crook, N., Binley, A., Knight, R., Robinson, D.A., Zarnetske, J., Haggerty, R., 2008. Electrical resistivity imaging of the architecture of substream sediments. Water Resour. Res. 44, W00D13. doi:https://doi.org/10.1029/2008 WR006968.

Deiana, R., Cassiani, G., Kemna, A., Villa, A., Bruno, V., Bagliani, A., 2007. An experiment of non-invasive characterization of the vadose zone via water injection and cross-hole time-lapse geophysical monitoring. Near. Surf. Geophys. 5 (3), 183–194. https://doi.org/10.3997/1873-0604.2006030.

Ebrahimi, F., Lenhard, R.J., Nakhaei, M., Nassery, H.R., 2019. An approach to optimize the location of LNAPL recovery wells using the concept of a LNAPL specific yield. Environ. Sci. Pollut. Res. 26 (28), 28714–28724. https://doi.org/10.1007/s11356-019-06052-7.

Faisal, A.A.H., Sulaymon, A.H., Khaliefa, Q.M., 2018. A review of permeable reactive barrier as passive sustainable technology for groundwater remediation. Int. J. Environ. Sci. Technol. 15, 1123–1138. https://doi.org/10.1007/s13762-017-1466-0.

Fan, D., Gilbert, E.J., Fox, T., 2017. Current state of in situ subsurface remediation by activated carbon-based amendments. J. Environ. Manag. 204, 793–803. https://doi.org/10.1016/j.jenvman.2017.02.014.

Flores-Orozco, A., Ciampi, P., Katona, T., Censini, M., Petrangeli Papini, M., Deidda, G.P., Cassiani, G., 2021. Delineation of hydrocarbon contaminants with multi-frequency complex conductivity imaging. Sci. Total Environ. 768, 144997 https://doi.org/10.1016/j.scitotenv.2021.144997.

Gatsios, E., García-Rincón, J., Rayner, J.L., McLaughlan, R.G., Davis, G.B., 2018. LNAPL transmissivity as a remediation metric in complex sites under water table fluctuations. J. Environ. Manag. 215, 40–48. https://doi.org/10.1016/j.jenvman.2018.03.026.

Ghosh, J., Tick, G.R., Akyol, N.H., Zhang, Y., 2019. A pore-scale investigation of heavy crude oil trapping and removal during surfactant-enhanced remediation. J. Contam. Hydrol. 223, 103471 https://doi.org/10.1016/j.jconhyd.2019.03.003.

Halihan, T., Albano, J., Comfort, S.D., Zlotnik, V.A., 2012. Electrical resistivity imaging of a permanganate injection during in situ treatment of RDX-contaminated groundwater. Groundw. Monit. Remed. 32 (1), 43–52. https://doi.org/10.1111/j.1745-6592.2011.01361.x.

Harte, P.T., Smith, T.E., Williams, J.H., Degnan, J.R., 2012. Time series geophysical monitoring of permanga- nate injections and in situ chemical oxidation of PCE, OU1 area, savage superfund site, Milford, NH, USA. J. Contam. Hydrol. 132, 58–74. https://doi.org/10.1016/j.jconhyd.2012.01.008.

Hort, R.D., Revil, A., Munakata-Marr, J., Mao, D., 2015. Evaluating the potential for quantitative monitoring of in situ chemical oxidation of aqueous-phase TCE using in-phase and quadrature electrical conductivity. Water Resour. Res. 51, 5239–5259. https://doi.org/10.1002/2014WR016868.

Hou, D., Al-Tabbaa, A., O'Connor, D., Hu, Q., Zhu, Y.G., Wang, L., Kirkwood, N., Ok, Y. S., Tsang, D.C.W., Bolan, N.S., Rinklebe, J., 2023. Sustainable remediation and redevelopment of brownfield sites. Nat. Rev. Earth Environ. 4 (4), 271–286. https://doi.org/10.1038/s43017-023-00404-1.

Huling, S.G., Ross, R.R., Meeker Prestbo, K., 2017. In situ chemical oxidation: permanganate oxidant volume design considerations. Groundw. Monit. R. 37, 78–86. https://doi.org/10.1111/gwmr.12195.

Ismail, R.E., Al-Raoush, R.I., Alazaiza, M.Y.D., 2023. The impact of water table fluctuation and salinity on LNAPL distribution and geochemical properties in the smear zone under completely anaerobic conditions. Environ. Earth Sci. 82, 368. https://doi.org/10.1007/s12665-023-11051-6.

Kuppusamy, S., Maddela, N.R., Megharaj, M., Venkateswarlu, K., 2020. Case studies on remediation of sites contaminated with Total petroleum hydrocarbons. In: Total Petroleum Hydrocarbons. Springer, Cham. https://doi.org/10.1007/978-3-030-24035-6_9.

Lari, K.S., Rayner, J.L., Davis, G.B., 2018. Towards characterizing LNAPL remediation endpoints. J. Environ. Manag. 224, 97–105. https://doi.org/10.1016/j.jenvman.2018.07.041.

Mackay, M.D., Cherry, J.A., 1989. Groundwater contamination: pump-and-treat remediation. Environ. Sci. Technol. 23, 630–636. https://doi.org/10.1021/es00064a001.

Mao, D., Revil, A., Hort, R.D., Munakata-Marr, J., Atekwana, E.A., Kulessa, B., 2015. Resistivity and self-potential tomography applied to groundwater remediation and

contaminant plumes: sandbox and field experiments. J. Hydrol. 530, 1–14. https://doi.org/10.1016/j.jhydrol.2015.09.031.
Mao, D., Lu, L., Revil, A., Zuo, Y., Hinton, J., Ren, Z.J., 2016. Geophysical monitoring of hydrocarbon-contaminated soils remediated with a bioelectrochemical system. Environ. Sci. Technol. 50 (15), 8205–8213. https://doi.org/10.1021/acs.est.6b00535.
Ossai, I.C., Ahmed, A., Hassan, A., Hamid, F.S., 2020. Remediation of soil and water contaminated with petroleum hydrocarbon: A review. Environ. Technol. Innov. 17, 100526 https://doi.org/10.1016/j.eti.2019.100526.
Pac, T.J., Baldock, J., Brodie, B., Byrd, J., Gil, B., Morris, K.A., Nelson, D., Parikh, J., Santos, P., Singer, M., Thomas, A., 2019. In situ chemical oxidation: lessons learned at multiple sites. Remediat. J. 29 (2), 75–91. https://doi.org/10.1002/rem.21591.
Pan, Y., Zhang, Q., Yu, Y., Tong, Y., Wu, W., Zhou, Y., Hou, W., Yang, J., 2021. Three-dimensional migration and resistivity characteristics of crude oil in heterogeneous soil layers. Environ. Pollut. 268, 115309 https://doi.org/10.1016/j.envpol.2020.115309.
Raji, W.O., Obadare, I.G., Odukoya, M.A., Johnson, L.M., 2018. Electrical resistivity mapping of oil spills in a coastal environment of Lagos, Nigeria. Arab. J. Geosci. 11, 1–9. https://doi.org/10.1007/s12517-018-3470-1.
Ranc, B., Faure, P., Croze, V., Simonnot, M.O., 2016. Selection of oxidant doses for in situ chemical oxidation of soils contaminated by polycyclic aromatic hydrocarbons (PAHs): A review. J. Hazard. Mater. 312, 280–297. https://doi.org/10.1016/j.jhazmat.2016.03.068.
Regenesis, 2023. Environmental Remediation Research. https://regenesis.com/en/. Accessed on 05/12/2023.
Revil, A., Coperey, A., Shao, Z., Florsch, N., Fabricius, I.L., Deng, Y., Delsman, J.R., Pauw, P.S., Karaoulis, M., de Louw, P.G.B., van Baaren, E.S., Dabekaussen, W., Menkovic, A., Gunnink, J.L., 2017. Complex conductivity of soils. Water Resour. Res. 53 (8), 7121–7147. https://doi.org/10.1002/2017WR020655.
Rubin, Y., Hubbard, S.S., 2006. Hydrogeophysics. Water Science and Technology Library, vol 50. Springer, Dordrecht, pp. 129-156. https://doi.org/10.1007/1-4020-3102-5_5.
Shao, S., Gao, C., Guo, X., Wang, Y., Zhang, Z., Yu, L., Tang, H., 2019. Mapping the contaminant plume of an abandoned hydrocarbon disposal site with geophysical and geochemical methods, Jiangsu, China. Environ. Sci. Pollut. Res. 26, 24645–24657. https://doi.org/10.1007/s11356-019-05780-0.
Sharma, S., Kostarelos, K., Lenschow, S., Christensen, A., de Blanc, P.C., 2020. Surfactant flooding makes a comeback: results of a full-scale, field implementation to recover mobilized NAPL. J. Contam. Hydrol. 230, 103602 https://doi.org/10.1016/j.jconhyd.2020.103602.
Teramoto, E.H., Pede, M.A.Z., Chang, H.K., 2020. Impact of water table fluctuations on the seasonal effectiveness of the pump-and-treat remediation in wet-dry tropical regions. Environ. Earth Sci. 79, 435. https://doi.org/10.1007/s12665-020-09182-1.
Tildy, P., Neducza, B., Nagy, P., Kanli, A.I., Hegymegi, C., 2017. Time lapse 3D geoelectric measurements for monitoring of in-situ remediation. J. Appl. Geophys. 136, 99–113. https://doi.org/10.1016/j.jappgeo.2016.10.037.
Tomlinson, D.W., Rivett, M.O., Wealthall, G.P., Sweeney, R.E., 2017. Understanding complex LNAPL sites: illustrated handbook of LNAPL transport and fate in the subsurface. J. Environ. Manag. 204, 748–756. https://doi.org/10.1016/j.jenvman.2017.08.015.
Tsai, Y.J., Wu, T.N., Lee, C.H., Lin, S.L., Tsai, W.H., 2021. Non-invasive survey technology for estimating the distribution of oxidant solution: A pilot injection study. J. Contam. Hydrol. 239, 103779 https://doi.org/10.1016/j.jconhyd.2021.103779.
Vereecken, H., Binley, A., Cassiani, G., Revil, A., Titov, K., 2006. Applied Hydrogeophysics. In: NATO Science Series, Vol 71. Springer, Dordrecht. https://doi.org/10.1007/978-1-4020-4912-5_1.
Wang, W.H., Hoag, G.E., Collins, J.B., Naidu, R., 2013. Evaluation of surfactant-enhanced in situ chemical oxidation (S-ISCO) in contaminated soil. Water Air Soil Pollut. 224, 1713. https://doi.org/10.1007/s11270-013-1713-z.
Xia, T., Dong, Y., Mao, D., Meng, J., 2021. Delineation of LNAPL contaminant plumes at a former perfumery plant using electrical resistivity tomography. Hydrogeol. J. 29, 1189–1201. https://doi.org/10.1007/s10040-021-02311-5.
Xia, T., Ma, M., Huisman, J.A., Zheng, C., Gao, C., Mao, D., 2023. Monitoring of in-situ chemical oxidation for remediation of diesel-contaminated soil with electrical resistivity tomography. J. Contam. Hydrol. 256, 104170 https://doi.org/10.1016/j.jconhyd.2023.104170.
Zhou, Z., Liu, X., Sun, K., Lin, C., Ma, J., He, M., Ouyang, W., 2019. Persulfate-based advanced oxidation processes (AOPs) for organic-contaminated soil remediation: A review. Chem. Eng. J. 372, 836–851. https://doi.org/10.1016/j.cej.2019.04.213.